HHS Public Access

Author manuscript

Neuropharmacology. Author manuscript; available in PMC 2021 March 15.

Published in final edited form as:

Neuropharmacology. 2020 March 15; 165: 107922. doi:10.1016/j.neuropharm.2019.107922.

Differential effects of HDAC inhibitors on PPN oscillatory activity in vivo

Veronica Bisagno, PhD[b], **Maria Alejandra Bernardi, PhD**[b], **Sara Sanz Blanco, PhD**[b], **Francisco J. Urbano, PhD**[c,#], **Edgar Garcia-Rill, PhD**[a,#]

[a]Center for Translational Neuroscience, University of Arkansas for Medical Sciences, Little Rock, AR, USA

[b]ININFA, Universidad de Buenos Aires, Buenos Aires, Argentina.

[c]IFIBYNE, DFBMC-CONICET, FCEN, Universidad de Buenos Aires, Buenos Aires, Argentina.

Abstract

The pedunculopontine nucleus (PPN) has long been known to be part of the reticular activating system (RAS) in charge of arousal and REM sleep. We previously showed that *in vitro* exposure to a HDAC Class I and II mixed inhibitor (TSA), or a specific HDAC class IIa inhibitor (MC 1568), decreased PPN gamma oscillations. Given the lack of information on systemic *in vivo* treatments on neuronal synaptic properties, the present study was designed to investigate the systemic effect of HDAC inhibitors (HDACi) on PPN rhythmicity. Rat pups were injected (acute, single dose) with TSA (4 or 20 mg/Kg), MC1568 (4 or 20 mg/Kg), or MS275 (20 or 100 mg/kg). Our results show that MC1568 (20 mg/Kg) reduced mean frequency of PPN oscillations at gamma band, while increasing mean input resistance (Rm) of PPN neurons. For TSA (4 and 20 mg/kg), we observed reduced mean frequency of oscillations at gamma band and increased mean Rm of PPN neurons. Systemic administration of 20 mg/Kg MC1568 and TSA effects on Rm were washed out after 60 minutes of *in vitro* incubation of PPN slices, suggesting an underlying functional recovery of PPN calcium-mediated gamma band oscillations over time. In addition, at a lower dose, 4 mg/Kg, MC1568 and TSA induced higher mean amplitude gamma oscillations. Blocking HDAC class I might not have deleterious effects on gamma activity, but, more importantly, the inhibition of HDAC class I (at 100mg/kg) increased gamma band oscillations. In conclusion, the present results *in vivo* validate our previous findings *in vitro* and further expand information on the effects

Corresponding author: E. Garcia-Rill, PhD, Director, Center for Translational Neuroscience, University of Arkansas for Medical Sciences, Slot 847, Little Rock, AR 72205, garciarilledgar@uams.edu.

[#]Authors equally contributed as senior authors.

Author contributions

Bisagno Conceptualization, design, data acquisition, figures

Bernardi New data, analysis, statistics, figure

Blanco New data, analysis, statistics, figure

Urbano Conceptualization, design, data acquisition, analysis, statistics, writing

Garcia-Rill Conceptualization, design, data analysis, wiring

Conflict of interest disclosure

Authors report no financial conflict of interest, or otherwise, related directly or indirectly to this study.

of HDAC inhibition on PPN rhythmicity. PPN neurons require normal activity of HDAC class IIa in order to oscillate at gamma band.

Bisagno et al. Graphical abstract.

Red arrows represent statistical significant inhibition. Blue arrows represent statistical significant enhancement. ~Represents absence of change.

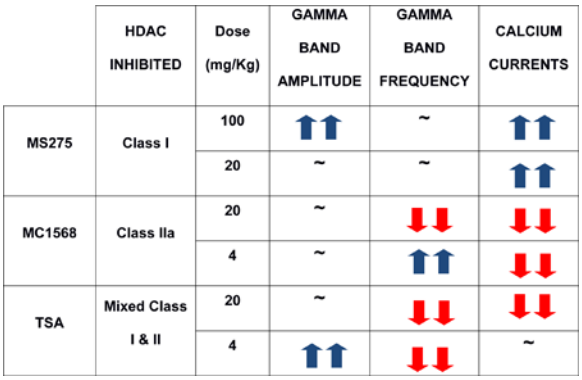

Our findings suggest that gamma oscillations in the PPN are finely tuned *in vivo* by the activity of HDAC class IIa. Sustained blocking of HDAC IIa blunted gamma band oscillations of PPN neurons. Blocking HDAC class I showed higher gamma band amplitudes. In conclusion, systemic administration of HDAC inhibitors might have either negative or positive effects on PPN rhythmicity depending of dose and group of HDAC affected.

Keywords

Arousal; calcium channels; Calcium currents; gamma oscillations; MC1568; MS275; neuroepigenetics; trichostatin A

1. Introduction

A wealth of evidence suggests that deregulation of gene transcription represents a key event in the pathogenesis of cancer and neurodegenerative diseases, and there is great interest in development of drugs able to restore transcriptional homeostasis (Belzil et al., 2016). To this end, inhibitors of histone deacetylases (HDACi) represent attractive candidates. HDAC enzymes regulate reversible acetylation of lysine residues of histones and non-histone proteins (Gallinari et al., 2007; Iyer et al., 2012), and are grouped in various classes [Class I (HDAC-1, −2, −3, −8), Class IIa (HDAC-4, −5, −7, −9), Class IIb (HDAC-6, −10), Class III (Sirtuins) and Class IV (HDAC-11); see Haberland et al., 2009 for review]. HDACs have been shown not only to deacetylate histones but also to target non-histone proteins involved in diverse signaling pathways. For example, Tubulin, p53, GATA, STAT3, and CBP among others were reported to be acetylated by histone acetyltransferases (HAT), suggesting that HDAC may regulate gene expression by deacetylation of these and other non-histone proteins (Singh et al., 2010).

In the context of cancer therapy, it has been suggested that normal cells are relatively resistant to treatment with HDACi, whereas tumor cells are more responsive (Qiu et al., 2000; Marks et al., 2001). Clinical studies using non-selective HDAC inhibitors induce unfavorable side effects in patients, so that it is essential to develop more isoform- and/or class–selective HDAC inhibitors, which would preserve significant anti-tumor activity and yet still improve patient outcome (Harada et al., 2016). HDAC inhibitors are proven anticancer therapeutics that also have potential for treatment of diseases affecting Central Nervous System like Alzheimer's disease, and Friedreich's ataxia (Millard et al., 2017). Other authors have investigated HDAC inhibition and brain ischemia (Lanzillotta et al., 2013; Formisano et al., 2015). It is thus imperative to understand the effect of specific HDAC inhibitors in the context of physiologically relevant neuronal processes such as intracellular [Ca^{2+}] dynamics and its associated membrane potential rhythmicity. However, the equilibrium between HDAC and HAT activities is a key to the epigenetic control of gene expression in normal tissue, therefore, HDACi treatment might interfere with and alter this balance. There is very limited information on preclinical studies aimed at the study of potential consequences of HDAC inhibition in normal subjects. Moreover, it is not clear how the loss of HDAC function affects healthy neurons. The pedunculopontine nucleus (PPN) has long been known to be part of the reticular activating system (RAS) in charge of arousal (Garcia-Rill, 2015; Garcia-Rill et al., 2016).

There are very few studies investigating the functional (i.e. behavioral) consequences of HDACi acute or chronic inhibition and it is a vacant area of study that warrants additional studies. In addition, behavioral consequences of HDACi will surely depend on drug doses and also likely be task-dependent. Chronic systemic MC1568 induced complex effects prompting early improvement of motor functions and greater time to fatigue in the SOD1-ALS mice that vanishes at later stages of disease (Buonvicino et al., 2018). Those effects did not correlate with a motorneuron sparing effect but with increased muscle electrical activity (Buonvicino et al., 2018), suggesting that HDACi were able to modulate neuromuscular physiology, well known to be finely tuned by both pre- and postsynaptic voltage-sensitive calcium channels. An HDACi not used in this study, valproic acid, has been described to improve motor and non-motor function in a Parkinson's disease genetic mouse model (Kim et al., 2019). Interestingly, MS-275 showed a clear neuroprotective effect in the post-ischemic mouse brain and improved neurological deficits (Lanzillota et al., 2013). On the other hand, neurological sequelae induced by HDACi include fatigue, status epilepticus, somnolence, and gait problems have also been described (Subramanian et al., 2010). Some of these side effects might be potentially driven by changes in HDAC/HAT balance.

We previously showed that *in vitro* exposure to the histone deacetylation Class I and II inhibitor TSA led to the elimination/reduction of high threshold, voltage-dependent Ca^{2+} channel-mediated oscillations, specifically in the gamma band range, but not lower frequencies. However, MS-275, a HDACi class I, did not alter oscillations. Given the lack of information on systemic *in vivo* treatments on neuronal synaptic properties, the present study was designed to investigate the systemic effects of HDACi *in vivo*. We designed the present experiments to test whether *in vivo* neuroepigenetic modulation of intrinsic properties of PPN neurons were time and dose dependent. We were able to replicate our

previous results using *in vitro* HDACi administration to PPN slices and expand our knowledge showing opposing roles of HDAC class I and IIa on PPN physiology.

2. Materials and methods

2.1. Animals

Rat pups (either sex, aged 9–13 days, 15–23 gr) from adult timed-pregnant Sprague-Dawley rats (280–350 gr, 6–10 pups per litter) used in this study were purchased from Charles River and housed at the Animal Facility at UAMS. Each litter was housed in individually ventilated cages with *ad libitum* access to water and food. All experimental protocols were approved by the Institutional Animal Care and Use Committee of the University of Arkansas for Medical Sciences (IACUC protocol #3906), in agreement with the National Institutes of Health guidelines for the care and use of laboratory animals.

2.2. Systemic in vivo treatments using HDACi

We injected (intraperitoneal injection; *i.p.*) rat pups with one of the HDACi (n=42 rats) or control solution (vehicle; n=28 rats). Animals were monitored regularly by researchers in charge of handling and injections. No exclusion criteria were pre-determined. None of the pups died from treatment or injection procedure. We minimized animal suffering by carefully injecting the animal, placing the injected pups in a warm and comfortable environment in their home cage. Researcher blindly and randomly injected pups, injections (morning or afternoon were balanced among groups). Researchers in charge of electrophysiological recordings, analysis of data, and statistical comparisons were blind to treatment schedules (i.e. the experimenter was unaware of the animal's group assignment). A simple randomization procedure was used to assign pups to either vehicle or HDACi treatment. Indeed, pups from every litter were assigned to vehicle or HDACi treatments randomly for every day of experiment.

HDACi *in vivo* administration (acute, single dose) was performed with the following agents: the selective HDAC class IIa inhibitor, MC1568 (4 or 20 mg/Kg, *i.p.*; Catalog #M1824; Sigma Aldrich, St. Louis, MO, USA or Catalog #4077; TOCRIS, MN, USA) [3-[5-(3-(3-Fluorophenyl)-3-oxopropen-1-yl)-1-methyl-1H-pyrrol-2-yl]-N-hydroxy-2-propenamide]; the HDAC class I & II inhibitor Trichostatin-A (4 or 20 mg/Kg, *i.p.*; Catalog #T8552; Sigma Aldrich, St. Louis, MO, USA or Catalog #1406; TOCRIS, MN, USA) [(2E,4E,6R)-7-(4-(Dimethylamino)phenyl)-N-hydroxy-4,6-dimethyl-7-oxo-2,4-heptadienamide]; and a HDAC class I inhibitor MS275 (20 or 100 mg/Kg, *i.p.*; Catalog #EPS002; Sigma Aldrich, St. Louis, MO, USA or Catalog #6208; TOCRIS, MN, USA) [Pyridin-3-yl)methyl 4-(2-aminophenylcarbamoyl) benzylcarbamate].

Stock solutions of HDACi used in this study were dissolved in DMSO and immediately stored at −30 ºC (Urbano et al., 2018). HDACi stock solutions were mixed with sterile saline solution (10% DMSO in sterile saline) prior to intraperitoneal injection. Vehicle groups received the same volume of DMSO+sterile saline (10% DMSO in sterile saline). Slices were obtained four hours after acute systemic administration of HDACi in order to allow drugs to be absorbed, reach maximum levels, and have additional time for pharmacodynamic

effects to occur. Previous studies showed that TSA is rapidly absorbed from the peritoneum and is detectable in plasma within 2 min with $t_{1/2}$ of 6.3 min (Sanderson et al., 2004). Also, preclinical pharmacology studies indicated that MS-275 showed a half-life ($t_{1/2}$) of approximately 1 hour, which was similar in rats, mice, and dogs (Acharya, 2005; Joksimovic et al., 2018). Other authors have previously reported that high plasma level of HDACi in cancer patients was maintained on average for at least 4 hr. (Dragovic et al., 1995). Thus, we decided to study effects on PPN rhythmicity 4 hr. after systemic administration of HDACi.

2.3. Slice preparation

Pups were anesthetized with ketamine (70 mg/kg, I.M.). Ketamine was approved by the Institutional Animal Care and Use Committee of the University of Arkansas for Medical Sciences and allowed us to induce analgesia, dissociation from the environment, and immobility of pups. When tail pinch reflex was absent, pups were killed by decapitation by a trained researcher and the brain was rapidly removed then cooled in oxygenated sucrose-artificial cerebrospinal fluid (sucrose-aCSF). The sucrose-aCSF consisted of (in mM): 233.7 sucrose, 26 $NaHCO_3$, 3 KCl, 8 $MgCl_2$, 0.5 $CaCl_2$, 20 glucose, 0.4 ascorbic acid, and 2 sodium pyruvate. Sagittal sections (400 μm) containing the PPN were cut and slices were allowed to equilibrate in normal aCSF at room temperature for 20 min. The aCSF was composed of (in mM): 117 NaCl, 4.7 KCl, 1.2 $MgCl_2$, 2.5 $CaCl_2$, 1.2 NaH_2PO_4, 24.9 $NaHCO_3$, and 11.5 glucose. Slices were recorded at 36˚C while perfused (1.5 ml/min) with oxygenated (95% O_2-5% CO_2) aCSF in an immersion chamber for patch clamp studies, as previously described (Kezunovic et al., 2011, 2012, 2013). During recordings, aCSF solution contained the following synaptic receptor antagonists: the selective NMDA receptor antagonist 2-amino-5-phosphonovaleric acid (APV, 40 μM; Catalog #A5282; Sigma Aldrich, St. Louis, MO, USA), the competitive AMPA/kainate glutamate receptor antagonist 6-cyano-7-nitroquinoxaline-2,3-dione (CNQX, 10 μM; Catalog #C239; Sigma Aldrich, St. Louis, MO, USA), the glycine receptor antagonist strychnine (STR, 10 μM; Catalog #S0532; Sigma Aldrich, St. Louis, MO, USA), the specific GABA-A receptor antagonist gabazine (GBZ, 10 μM; Catalog #S106; Sigma Aldrich, St. Louis, MO, USA), and the nicotinic receptor antagonist mecamylamine (MEC, 10 μM; Catalog #M9020; Sigma Aldrich, St. Louis, MO, USA), collectively referred to here as synaptic blockers (SB) plus tetrodotoxin (TTX; 3 μM; Catalog #554412; Sigma Aldrich, St. Louis, MO, USA; Catalog #T550, Alomone labs., Israel, or Catalog #1069; TOCRIS, MN, USA).

2.4. Whole-cell patch-clamp recordings

Differential interference contrast optics was used to visualize neurons using an upright microscope (Nikon FN-1, Nikon, USA, USA). Whole-cell recordings were performed using borosilicate glass capillaries pulled on a P-97 puller (Sutter Instrument Company, Novato, CA, USA), and filled with a high-K^+ intracellular solution, designed to mimic the intracellular electrolyte concentration, of (in mM): 110 K^+-Gluconate; 30 KCl; 10 Hepes; 10 Na_2 phosphocreatine; 0.2 EGTA; 2 Mg-ATP; 0.5 Li-GTP; 1 $MgCl_2$. Osmolarity was adjusted to ~270–290 mOsm and pH to 7.3. The pipette resistance was 2–5 MΩ. All recordings were made using a Multiclamp 700B amplifier (Molecular Devices, Sunnyvale, CA, USA) in both current and voltage clamp mode. Digital signals were low-pass filtered at 2 kHz and digitized at 5 kHz using a Digidata-1440A interface and pClamp10 software

(Molecular Devices, CA, USA). We used 1.5 sec-long depolarizing current ramps to study membrane potential oscillations. Current ramps allow us to gradually change membrane potential from resting values up to 0 mV in current clamp mode (Kezunovic et al., 2011, 2012, 2013).

The recorded neurons were localized in the *pars compacta* in the posterior PPN, which is easily identified in sagittal sections of the brainstem (Kezunovic et al., 2011; Simon et al., 2010). This area of the PPN has been shown to have the highest density of cells (Wang and Morales 2009; Ye et al., 2010). We first identified PPN neurons by cell type as previously described (Garcia-Rill et al., 2007, 2008; Simon et al., 2010), although all cell types showed gamma band oscillations when depolarized using current ramps during bath-applied SB +TTX via a peristaltic pump (Cole-Parmer, Vernon Hills, IL, USA) (Kezunovic et al., 2011; Urbano et al., 2018, 2019).

Gigaseal formation and further access to the intracellular neuronal compartment was achieved in voltage-clamp mode. Within a short time after rupturing the membrane, the intracellular solution reached equilibrium with the pipette solution without significant changes in either series resistance (ranging 7–12 MΩ) or membrane capacitance values. Membrane input resistance (Rm) was calculated using square hyperpolarizing current pulses in current-clamp mode (−300 pA, 500 msec long). Since Rm was previously described to be altered by HDACi *in vitro* application (Urbano et al., 2018; 2019), in this study we plotted the time course of Rm values recorded in PPN slices at different *in vitro* incubation times in order to monitor HDACi washout. Individual Rm values were well fitted to the following exponential decay function: $Rm=(Rm)o + a*\exp^{(-time/\tau)}$.

In addition to oscillation recordings, voltage-dependent Ca^{2+} currents (I_{Ca}) were studied using a high-Cs^{+}/QX-314 pipette solution (in mM: 110 $CsMeSO_3$, 40 Hepes, 10 TEA-Cl, 12 Na_2-phosphocreatine, 0.5 EGTA, 2 Mg-ATP, 0.5 Li-GTP, and 1 $MgCl_2$. pH was adjusted to 7.3 with CsOH). Cesium and TEA-Cl (Sigma Aldrich, St. Louis, MO, USA) are well known potassium channel blockers. I_{Ca} were recorded in the presence of extracellular synaptic receptor antagonists (Kezunovic et al., 2011, 2012, 2013; Urbano et al., 2019), and the sodium and potassium channel blockers tetrodotoxin (TTX, 3 μM; TOCRIS, MN, USA) and TEA-Cl (25 mM), respectively. Square voltage steps (100 msec long) were used to generate PPN neuronal I_{Ca} from a holding potential of −50 mV, and then depolarized up to 40 mV. Setting the holding potential at −50 mV allowed us to inactivate T-type Ca^{2+} channels, while allowing normal activation of high-threshold P/Q- and N-type Ca^{2+} channels that have been described by our group to mediate intrinsic gamma oscillations (Kezunovic et al., 2011, 2012, 2013; D'Onofrio et al., 2015; Urbano et al., 2018, 2019). Both series resistance and liquid junction potential were compensated (>14 kHz correction bandwidth; equivalent to <10 μsec lag).

2.5. Data Analysis and Statistical Comparisons

Off-line analyses were performed using Clampfit software (Molecular Devices, Sunnyvale, CA, USA). Peak oscillatory amplitude was analyzed by first filtering each ramp recording and measuring the three highest amplitude oscillations to derive a mean amplitude induced during each ramp. The mean peak frequency of the same three oscillations was filtered and

measured to derive a mean frequency of oscillations during the three highest amplitude oscillations in each ramp. The power of each frequency was also analyzed by composing a power spectrum for the frequencies in the entire ramp (bandpass filtered; high pass 10 Hz, low pass 100 Hz), giving a measure of peak power for frequency (Urbano et al., 2018, 2019). Comparisons between groups were carried out using OriginPro 9.1.0 (Originlab.com, MA, USA). Normality and equal variance test were performed prior to ANOVA comparisons using Origin Pro 9.1.0. No sample calculation was performed. Data values that showed more than 2 SD from the mean were excluded. F values and degrees of freedom are reported for all linear regression ANOVAs. Differences were considered significant at values of $p \leq 0.05$. All results are presented as mean ± S.E.M.

3. Results

In the present study, we characterized the effects of systemically administered HDACi on PPN neuronal rhythmicity. We injected (intraperitoneal injection; *i.p.*) rat pups with one of the HDACi (n=42 rats) or control solution (vehicle; n=28 rats). Recordings of gamma band oscillations in PPN neurons (total number of cells studied, n=380) were performed using slices at 36 °C in the presence of synaptic blockers (SB) and TTX. We quantified and compared membrane resistance (Rm), amplitude and frequency oscillations of PPN neurons from HDACi treated *versus* control animals.

There are very few studies using *in vivo* systemic HDACi administration. We selected the dose range used in the present study based on previous reports showing no toxicity and good tolerability of HDACi administered *i.p.* For example, Buonvicino et al. (2018) showed that systemic treatment with MC1568 (40 mg/kg, *i.p.*) caused improvement of motor performance in the SOD1-ALS mice. In addition, systemic MC1568 showed neuroprotective effects in prefrontal cortex tissue from rats exposed to mercury toxicity (Guida et al., 2016). Shen et al. (2017) reported that TSA (30 and 60 mg/kg *i.p.*) induced an improvement of learning and memory impairments in APPswe/PS1dE9 mice, suggesting not only good tolerability but some degree of brain barrier penetration in order to show improvement at the CNS level. Dalgard et al. (2008) demonstrated that MS-275 (20mg/kg, *i.p.*) is a well-tolerated and highly effective treatment for mouse retinoblastoma. Therefore, we selected an initial dose of 20 mg/kg for all the HDACi tested: Trichostatin-A (TSA), MC1568 and MS-275. We initially tested whether HDACi systemic *in vivo* effects were washed out through *in vitro* incubation and recording time of PPN neurons in slices. Based on our previously described increase of membrane resistance (Rm) values after *in vitro* application of MC1568 (Urbano et al., 2018), we obtained Rm values from PPN neurons recorded *in vitro* at different times after *in vivo* HDACi (Figure 1). Two-way ANOVA showed statistically significant interactions between time (<60 min versus >60 min periods) and treatment (Vehicle versus MC1568, 20 mg/Kg, i.p.) for Rm ($F(1,53)=5.25$, $p=0.025$). In addition, Two-way ANOVA analysis of recorded Rm after TSA *in vivo* treatment showed a statistically significant interaction between time and treatment ($F(1,70)=4.8$, $p=0.03$).

In PPN neurons from MC1568 (20 mg/Kg) treated animals, Rm values were initially higher followed by a continued reduction until steady state values were achieved (Figure 1A, red triangles). The time course of Rm reduction was fitted to an exponential decay (Figure 1A,

red dotted line). Mean Rm values were significantly higher at <60 minutes compared to longer times (Figure 1B). Similarly, TSA (20 mg/Kg) effects on Rm were washed out over time following an exponential decay (Figure 1C), presenting significantly higher Rm values before vs after 60 min (Figure 1D).

No time dependent changes in Rm were observed in PPN neurons from vehicle (Figure 1E, F) treated rats. Thus, in this work we continued using recording times below 60 minutes after cutting slices in order to characterize maximal effects of systemic effects of HDACi on PPN rhythmicity.

3.1. In vivo treatment of HDAC class IIa with MC1568 decreased PPN gamma oscillations

Recordings of PPN neurons for less than 60 minutes showed that MC1568 20 mg/kg (*i.p.*) treatment reduced gamma band oscillations in PPN neurons (Figure 2A-D). MC1568 elicited a dose-dependent reduction of mean frequency of oscillations in PPN neurons (Figure 2E). We then tested a lower dose of MC1568 (Figure 2E, dashed red bar; 4 mg/Kg, *i.p.*) which enhanced, while 20 mg/Kg reduced (Figure 2E, solid red bar), mean frequency of gamma band oscillations (One way ANOVA; *post hoc Tukey's test*; $p<0.05$). No statistically different oscillation amplitudes were observed when comparing all groups (Figure 2F, One way ANOVA; *post hoc Tukey's test*; $p>0.05$). However, higher Rm values were observed in PPN neurons only after 20 mg/Kg MC1568 treatment (Figure 2G; One way ANOVA; *post hoc Tukey's test*; $p<0.05$). Thus, we observed a dose-dependent effect of systemic MC1568 on gamma band oscillatory activity in the PPN.

3.2. In vivo treatment with the HDAC class I and II inhibitor TSA showed a mixed pattern of effects on PPN gamma frequency of oscillations

Systemic administration of TSA (20 mg/Kg; *i.p.*) also reduced gamma band activity of PPN when recorded less than 60 min after slicing (Figure 3A-D). TSA significantly reduced the frequency of oscillations at both low (4 mg/Kg, *i.p.*) and high (20 mg/Kg, *i.p.*) doses (Figure 3E; One way ANOVA; *post hoc Tukey's test*; $p<0.05$), while higher amplitudes were observed only after 4 mg/Kg treatment (Figure 3F; One way ANOVA; *post hoc Tukey's test*; $p<0.05$). Mean Rm values were significantly higher at low (4 mg/Kg, *i.p.*) and high (20 mg/Kg, *i.p.*) doses (Figure 3G; One way ANOVA; *post hoc Tukey's test*; $p<0.05$).

When administered at a 20 mg/Kg dose, TSA mimicked the effects with MC1568 on PPN rhythmicity after their blockage of class IIa HDAC. However, 4 mg/Kg TSA enhanced gamma band oscillation amplitude. This paradoxical effect suggested that low dose TSA-mediated antagonism of other HDAC classes might have a dis-inhibitory role on gamma band oscillations.

3.3. In vivo treatment with the HDAC class I inhibitor MS275 enhanced gamma band PPN oscillations at high doses.

Systemic treatment with MS275 (20 mg/Kg) induced no significant changes in oscillation amplitudes. However, higher doses of MS275 enhanced the amplitude of TTX-insensitive, gamma oscillations in PPN less than 60 min after slicing (Figure 4A, B). Neither using the lower dose of 20 mg/Kg nor the 100 mg/Kg dose of MS275 affected the mean frequency of

gamma oscillations (Figure 4C; One way ANOVA; *post hoc Tukey's test*; p>0.05), while amplitude was significantly higher for 100 mg/Kg MS275 (Figure 4D; One way ANOVA; *post hoc Tukey's test*; p<0.05). No significant differences were observed for Rm (Figure 4E; One way ANOVA; *post hoc Tukey's test*; p>0.05). Therefore, *in vivo* inhibition of HDAC class I with a high dose of MS275 induced a rebound effect on the amplitude of gamma band oscillations in the PPN.

3.4. In vivo treatment with several HDACi prompted biphasic changes in PPN neuron Ca^{2+} current (I_{Ca}) density

First, we compared the effects of 20 mg/Kg (*i.p.*) MC1568, TSA, and MS275 on Ca^{2+} current density (I_{Ca}) (Figure 5A). Figure 5B shows that MC1568 and TSA (20 mg/Kg) blocked PPN I_{Ca} by a similar percentage (~50% reduction; One way ANOVA, *post hoc Tukey's test*; P<0.05). Strikingly, MS275 (20 mg/Kg) enhanced I_{Ca} current density in PPN neurons (Figure 5B, ~40% increase; One way ANOVA, *post hoc Tukey's test*; p<0.05). At a lower dose (4 mg/Kg), only MC1568 reduced I_{Ca} (Figure 5C, ~30% increase; One way ANOVA, *post hoc Tukey's test*; p<0.05). Low dose TSA (4 mg/Kg) did not affect I_{Ca} (Figure 4C, One way ANOVA, *post hoc Tukey's test*; p>0.05). On the other hand, MS275 (100 mg/Kg) treatment induced higher I_{Ca} mean density values (Figure 5C, ~45% increase; One way ANOVA, *post hoc Tukey's test*; p<0.05), to a similar magnitude as previously observed in MS275 20 mg/Kg treated PPN neurons (One way ANOVA, *post hoc Tukey's test*; p>0.05).

3.5. Effects of co-administration of HDAC class I and class IIa on PPN gamma oscillations

An additional experiment was performed to investigate co-administration of specific inhibitor of HDAC class I, MS275 (100 mg/Kg; *i.p.*), and the HDAC class Iia inhibitor, MC1568 (20 mg/Kg; *i.p.*). Figure 6A shows that when both HDAC class I and class Iia are blocked by specific antagonists, the previously reported effect of MS275 at a high dose (100 mg/Kg; *i.p.*), i.e. increased gamma band amplitude, was no longer present. Indeed, mean amplitudes were significantly lower when MC1568 (20 mg/Kg) was co-administrated with 100 mg/Kg MS275 (Figure 6B; One way ANOVA; *post hoc Tukey's test*; p<0.05). No significant differences were observed on either Rm or frequency of gamma oscillations (Figure 6C, D; One way ANOVA; *post hoc Tukey's test*; p>0.05). These results suggest that, as mentioned above, blocking HDAC class IIa produced detrimental effects on gamma band oscillations. Also, these results suggest a fine physiological balance between HDAC class I and IIa activation regarding PPN rhythmicity.

4. Discussion

We previously reported that *in vitro* exposure to the HDACi TSA decreased PPN oscillations in the gamma range, but not lower frequencies, and that Ca^{2+} currents (I_{Ca}) were reduced by TSA, especially in cells with P/Q-type channels, suggesting that bath application of HDACi could change PPN rhythmicity (Urbano et al., 2018). In addition, our group has previously shown augmented and reduced protein expression within minutes after TSA exposure in the presence of synaptic blockers and TTX (Byrum et al., 2019). Changes in rhythmicity and protein expression induced by HDACi on the PPN occurred within minutes, suggesting that

HDAC are potentially able to target not only histones but also non-histone proteins (Gallinari et al., 2007; Choudhary et al., 2009; Iyer et al., 2012). Indeed, our results might be explained by decreased deacetylation of histones, which might produce changes in gene expression, or changes in the deacetylation of other protein targets (both at the nuclear and cytoplasmic compartments, i.e., CaMKII (Choudhary et al., 2009), or F-actin polymerization/depolymerization (Byrum et al., 2019; Urbano et al., 2019).

However, in the clinical setting, HDACi are administered systemically. In the present study, we present evidence suggesting that acute systemic treatment with HDACi also altered PPN oscillatory activity depending on which class of HDAC was blocked, and that the effect manifested in a dose-dependent manner. First, it needs to be mentioned that our study showed clear effects on Rm, supporting the central idea that HDACi can reach the PPN and significantly influence intrinsic membrane properties in these neurons. Rm has been described by our group as a key intrinsic parameter linked to the blocking of voltage-dependent calcium channels in the presence of HDACi (Urbano et al., 2018). Systemic administration of 20 mg/Kg MC1568 and TSA effects on Rm were washed out after 60 minutes of *in vitro* incubation of PPN slices, suggesting that underlying functional recovery of PPN calcium-mediated gamma band oscillations over time. Therefore, our results point out that the effects induced by HDACi described here on PPN rhythmicity are not permanent but transient.

Furthermore, our study showed: 1) HDAC class IIa inhibition with MC1568 blunted gamma band oscillations in the PPN. High doses of MC1568 (20 mg/Kg) reduced mean frequency of PPN oscillations at gamma band, while increasing mean input resistance of PPN (Rm) neurons. A lower dose, 4 mg/Kg, of MC1568 showed opposite effects, increasing mean frequency of oscillations. Both doses reduced current density of calcium currents. We concluded that inhibition of HDAC IIa reduced oscillations and membrane channels were closed (leading to increased Rm). 2) Systemic effects of HDACi on gamma oscillations in PPN neurons were washed out during *in vitro* incubation of PPN slices. That is, maximal effects were observed over the <60 min period after cutting slices, but not thereafter. 3) A high dose of the HDAC class I and II mixed inhibitor TSA (20 mg/Kg) reduced mean frequency of oscillations at gamma band and increased mean Rm of PPN neurons. However, a lower dose of TSA (4 mg/Kg) we show an increase of the mean amplitude of gamma oscillations while showing similar effects on frequency and Rm as the 20 mg/Kg dose. Our result suggest that the lower dose increased the flow of Ca^{2+} while still closing some channels, perhaps N-type channels. 4) HDAC class I inhibition with a dose of MS275 (20 mg/Kg) did not affect gamma band oscillations at all in the PPN, therefore, we decided to test a higher dose. MS275 at 100 mg/Kg, on the other hand, increased mean amplitude of gamma band oscillations. Both doses equally enhanced current density of Ca^{2+} currents. Interestingly, it appears that blocking HDAC class I might not have deleterious effects on gamma activity, but, more importantly, the inhibition of HDAC class I (at a higher dose) could induce positive effects on gamma band oscillations within PPN. As far as we know, this is the first study showing distinctive and differential (positive or negative) effects on the physiology of PPN neurons based on the type and dose of HDAC inhibition.

Co-administration of MC1568 (20 mg/Kg) blunted the effects of MS275 (100 mg/Kg) on gamma band mean amplitude supporting the fact that blocking HDAC class IIa is detrimental to gamma band oscillation, even to the increase in gamma band mediated by a high dose of MS275.

Our results suggest the existence of a baseline balance of class I/class IIa activity in the PPN, under normal conditions. It has been reported that HDAC class I (for example, HDAC2) are involved in the regulation of potassium ion channel subunit 1.2 (Kv1.2) in the dorsal root ganglion (DRG), influencing neuronal excitability in a model of neuropathic pain (Li et al., 2019). We thus can speculate that some of the effects described here are due to potassium ion channel involvement in neuronal oscillations. In keeping with this suggestion, we showed that rectifier-like potassium channels are involved in the repolarizing phase of gamma oscillations in PPN neurons (Kezunovic et al., 2011), so that some of the effects on amplitude may be related to influences on such potassium channels.

Our results also point out that selective HDACi might be potentially beneficial to PPN physiology and/or several pathological conditions (that manifest problems with arousal and sleep-wake cycles) that rely on PPN integrity. It needs to be noted that targeting HDAC class I inhibition (using MS-275) proved to be beneficial in different animal models of depression, as well as fear, anxiety, and trauma-related psychiatric disorders (Singewald et al., 2015). Further studies are needed in order to clarify the physiological role of each one of the HDAC family members on PPN physiological functions and its emergent properties. Additionally, it would be interesting to test if these effects of HDACi on oscillations are exclusive to PPN neurons or extend to oscillatory mechanisms in different neuronal circuits, i.e. thalamocortical oscillations. Data on the effects of HDACi on synaptic properties of normal tissue is very limited, therefore, those issues should continue to be examined in relation to the compounds tested here and other clinically relevant HDACi.

5. Conclusions

Present results *in vivo* validate our previous findings *in vitro* and further expand information on the effects of HDAC class I inhibition on PPN rhythmicity. PPN neurons require normal activity of HDAC class IIa in order to oscillate at gamma band. Further, inhibition of HDAC class I could enhance PPN oscillation amplitude showing that the administration of HDACi might have either negative or positive effects on PPN rhythmicity depending of dose and group of HDAC affected.

Acknowledgments and Funding Sources

All experiments were conducted in compliance with the ARRIVE guidelines. This work was supported by National Institutes of Health (NIH) award P30 GM110702 from the IDeA program at NIGMS to the CTN. In addition, this work was supported by grants from FONCYT-Agencia Nacional de Promoción Científica y Tecnológica; Préstamo BID 1728 OC.AR. PICT-2016–1728, and PICT-2018–1744 and UBACYT 2014–2017 #20120130101305BA (to Dr. Urbano); FONCYT-Agencia Nacional de Promoción Científica y Tecnológica; Préstamo BID 1728 OC.AR. PICT 2015–2594 (to Dr. Bisagno).

Abbreviations:

aCSF	artificial cerebrospinal fluid

APV	2-amino-5-phosphonovaleric acid
GBZ	gabazine
CNQX	6-cyano-7-nitroquinoxaline-2,3-dione
DMSO	dimethyl sulfoxide
HDAC	histone deacetylases
HDACi	inhibitors of histone deacetylases
i.p.	intraperitoneal
I_{Ca}	calcium currents
MC1568	[3-[5-(3-(3-Fluorophenyl)-3-oxopropen-1-yl)-1-methyl-1H-pyrrol-2-yl]-N-hydroxy-2-propenamide]
MEC	mecamylamine
MS275	[Pyridin-3-yl)methyl 4-(2-aminophenylcarbamoyl)benzylcarbamate]
PPN	pedunculopontine nucleus
Rm	membrane input resistance
QX-314	N-Ethyllidocaine chloride;
SB	Synaptic blockers
STR	strychnine
TEA-Cl	tetraethylammonium chloride
TSA	Trichostatin-A or [(2E,4E,6R)-7-(4-(Dimethylamino)phenyl)-N-hydroxy-4,6-dimethyl-7-oxo-2,4heptadienamide]
TTX	tetrodotoxin

References

Acharya MR, 2005 Clinical Pharmacology of MS-275, A Histone Deacetylase Inhibitor. https://scholarscompass.vcu.edu/etd/index.54.html, year_2005.Thesis/Dissertation.

Belzil VV, Katzman RB, Petrucelli L. 2016 ALS and FTD: an epigenetic perspective. Acta Neuropathol. 132(4), 487–502. 10.1007/s00401-016-1587-4. [PubMed: 27282474]

Buonvicino D, Felici R, Ranieri G, Caramelli R, Lapucci A, Cavone L, Muzzi M, Di Pietro L, Bernardini C, Zwergel C, Valente S, Mai A, Chiarugi A, 2018 Effects of Class II-Selective Histone Deacetylase Inhibitor on Neuromuscular Function and Disease Progression in SOD1-ALS Mice. Neuroscience. 379, 228–238. 10.1016/j.neuroscience.2018.03.022. [PubMed: 29588251]

Byrum SD, Washam CL, Tackett AJ, Garcia-Rill E, Bisagno V, Urbano FJ 2019 Proteomic measures of gamma oscillations. Heliyon. 5(8), e02265. 10.1016/j.heliyon.2019.e02265.

Choudhary C, Kumar C, Gnad F, Nielsen ML, Rehman M, Walther TC, Olsen JV, Mann M. 2009 Lysine acetylation targets protein complexes and co-regulates major cellular functions. Science. 325(5942), 834–840. doi: 10.1126/science.1175371. [PubMed: 19608861]

Dalgard CL, Van Quill KR, O'Brien JM, 2008 Evaluation of the in vitro and in vivo antitumor activity of histone deacetylase inhibitors for the therapy of retinoblastoma. Clin. Cancer Res. 14(10), 3113–3123. 10.1158/1078-0432.CCR-07-4836. [PubMed: 18483379]

D'Onofrio S, Kezunovic N, Hyde JR, Luster B, Messias E, Urbano FJ, Garcia-Rill E, 2015 Modulation of gamma oscillations in the pedunculopontine nucleus (PPN) by neuronal calcium sensor protein-1 (NCS-1): relevance to schizophrenia and bipolar disorder. J. Neurophysiol. 113, 709–719. 10.1152/jn.00828.2014. [PubMed: 25376789]

Dragovic J, Kim SH, Brown SL, Kim JH, 1995 Nicotinamide pharmacokinetics in patients. Radiother. Oncol. 36, 225–228. [PubMed: 8532910]

Formisano L, Guida N, Valsecchi V, Cantile M, Cuomo O, Vinciguerra A, Laudati G, Pignataro G, Sirabella R, Di Renzo G, Annunziato L, 2015 Sp3/REST/HDAC1/HDAC2 Complex Represses and Sp1/HIF-1/p300 Complex Activates ncx1 Gene Transcription, in Brain Ischemia and in Ischemic Brain Preconditioning, by Epigenetic Mechanism. J. Neurosci. 35(19), 7332–7348. 10.1523/JNEUROSCI.2174-14.2015. [PubMed: 25972164]

Gallinari P, Di Marco S, Jones P, Pallaoro M, Steinkühler C, 2007 HDAC, histone deacetylation and gene transcription: from molecular biology to cancer therapeutics. Cell Res. 17(3), 195–211. 10.1038/sj.cr.7310149 [PubMed: 17325692]

Garcia-Rill E, 2015 Waking and the Reticular Activating System. Academic Press, New York, eBook ISBN: 9780128016329, Hardcover ISBN 9780128013854, pp. 330.

Garcia-Rill E, Heister DS, Ye M, Charlesworth A, Hayar A, 2007 Electrical coupling: novel mechanism for sleep-wake control. Sleep 30, 1405–1414. 10.1093/sleep/30.11.1405. [PubMed: 18041475]

Garcia-Rill E, Charlesworth A, Heister D, Ye M, Hayar A, 2008 The developmental decrease in REM sleep: The role of transmitters and electrical coupling. Sleep 31, 673–690. 10.1093/sleep/31.5.673. [PubMed: 18517037]

Garcia-Rill E, Luster B, D'Onofrio S, Mahaffey S, Bisagno V, Urbano FJ, 2016 Implications of gamma band activity in the pedunculopontine nucleus. J. Neural. Transm. (Vienna). 123(7), 655–665. 10.1007/s00702015-1485-2. [PubMed: 26597124]

Guida N, Laudati G, Mascolo L, Cuomo O, Anzilotti S, Sirabella R, Santopaolo M, Galgani M, Montuori P, Di Renzo G, Canzoniero LM, Formisano L, 2016 MC1568 Inhibits Thimerosal-Induced Apoptotic Cell Death by Preventing HDAC4 Up-Regulation in Neuronal Cells and in Rat Prefrontal Cortex. Toxicol. Sci. 154(2), 227–240. 10.1093/toxsci/kfw157 [PubMed: 27660204]

Haberland M, Montgomery RL, Olson EN, 2009 The many roles of histone deacetylases in development and physiology: implications for disease and therapy. Nat. Rev. Genet. 10, 32–42. 10.1038/nrg2485 [PubMed: 19065135]

Harada T, Hideshima T, Anderson KC, 2016 Histone deacetylase inhibitors in multiple myeloma: from bench to bedside. Int. J. Hematol. 104(3), 300–309. doi: 10.1007/s12185-016-2008-0. [PubMed: 27099225]

Joksimovic SM, Osuru HP, Oklopcic A, Beenhakker MP, Jevtovic-Todorovic V, Todorovic SM, 2018 Histone Deacetylase Inhibitor Entinostat (MS-275) Restores Anesthesia-induced Alteration of Inhibitory Synaptic Transmission in the Developing Rat Hippocampus. Mol. Neurobiol. 55(1), 222–228. 10.1007/s12035-017-0735-8. [PubMed: 28840475]

Kezunovic N, Urbano FJ, Simon C, Hyde J, Smith K, Garcia-Rill E, 2011 Mechanism behind gamma band activity in the pedunculopontine nucleus (PPN). Eur. J. Neurosci. 34, 404–415. 10.1111/j.14609568.2011.07766.x. [PubMed: 21722210]

Kezunovic N, Hyde J, Simon C, Urbano FJ, Williams DK, Garcia-Rill E, 2012 Gamma band activity in the developing parafascicular nucleus (Pf). J. Neurophysiol. 107, 772–784. 10.1152/jn.00677.2011. [PubMed: 22090455]

Kezunovic N, Hyde J, Goitia B, Bisagno V, Urbano FJ, Garcia-Rill E, 2013 Muscarinic modulation of high frequency oscillations in pedunculopontine neurons. Front. Neurol. 4, 176 10.3389/fneur.2013.00176. [PubMed: 24223570]

Kim T, Song S, Park Y, Kang S, Seo H. (2019). HDAC Inhibition by Valproic Acid Induces Neuroprotection and Improvement of PD-like Behaviors in LRRK2 R1441G Transgenic Mice. Exp. Neurobiol. 28(4):504–515. doi: 10.5607/en.2019.28.4.504. [PubMed: 31495079]

Lanzillotta A, Pignataro G, Branca C, Cuomo O, Sarnico I, Benarese M, Annunziato L, Spano P, Pizzi M (2013) Targeted acetylation of NF-kappaB/RelA and histones by epigenetic drugs reduces post-ischemic brain injury in mice with an extended therapeutic window. Neurobiol. Dis. 49, 177–189. 10.1016/j.nbd.2012.08.018. [PubMed: 22971966]

Li Z, Guo Y, Ren X, Rong L, Huang M, Cao J, Zang W, 2019 HDAC2, but not HDAC1, regulates Kv1.2 expression to mediate neuropathic pain in CCI rats. Neuroscience 408, 339–348. 10.1016/j.neuroscience.2019.03.033. [PubMed: 31022463]

Iyer A, Fairlie DP, Brown L, 2012. Lysine acetylation in obesity, diabetes and metabolic disease. Immunol. Cell Biol. 90(1), 39–46. 10.1038/icb.2011.99. [PubMed: 22083525]

Marks P, Rifkind RA, Richon VM, Breslow R, Miller T, Kelly WK, 2001 Histone deacetylases and cancer: causes and therapies. Nat. Rev. Cancer. 1(3), 194–202. 10.1038/35106079. [PubMed: 11902574]

Millard CJ, Watson PJ, Fairall L, Schwabe JWR 2017Targeting Class I Histone Deacetylases in a "Complex" Environment. Trends Pharmacol. Sci. 38(4), 363–377. doi: 10.1016/j.tips.2016.12.006. [PubMed: 28139258]

Qiu L, Burgess A, Fairlie DP, Leonard H, Parsons PG, Gabrielli BG, 2000 Histone deacetylase inhibitors trigger a G2 checkpoint in normal cells that is defective in tumor cells. Mol. Biol. Cell. 11(6), 2069–2083. 10.1091/mbc.11.6.2069 [PubMed: 10848630]

Sanderson L, Taylor GW, Aboagye EO, Alao JP, Latigo JR, Coombes RC, Vigushin DM, 2004 Plasma pharmacokinetics and metabolism of the histone deacetylase inhibitor trichostatin a after intraperitoneal administration to mice. Drug Metab. Dispos. 32(10), 1132–1138. 10.1124/dmd.104.000638 [PubMed: 15269190]

Shen L, Han B, Geng Y, Wang J, Wang Z, Wang M, 2017 Amelioration of cognitive impairments in APPswe/PS1dE9 mice is associated with metabolites alteration induced by total salvianolic acid. PLoS One. 12(3), e0174763. 10.1371/journal.pone.0174763.

Simon C, Kezunovic N, Ye M, Hyde J, Hayar A, Williams DK, Garcia-Rill E, 2010 Gamma band unit activity and population responses in the pedunculopontine nucleus. J. Neurophysiol. 104(1), 463–474. doi: 10.1152/jn.00242.2010. [PubMed: 20463196]

Singewald N, Schmuckermair C, Whittle N, Holmes A, Ressler KJ, 2015 Pharmacology of cognitive enhancers for exposure-based therapy of fear, anxiety and trauma-related disorders. Pharmacol. Ther. 149, 150–190. 10.1016/j.pharmthera.2014.12.004 [PubMed: 25550231]

Singh BN, Zhang G, Hwa YL, Li J, Dowdy SC, Jiang SW, 2010 Nonhistone protein acetylation as cancer therapy targets. Expert. Rev. Anticancer Ther. 10(6), 935–954. 10.1586/era.10.62. [PubMed: 20553216]

Subramanian S, Bates SE, Wright JJ, Espinoza-Delgado I, Piekarz RL, 2010 Clinical Toxicities of Histone Deacetylase Inhibitors. Pharmaceuticals (Basel). 3(9), 2751–2767. 10.3390/ph3092751 [PubMed: 27713375]

Urbano FJ, Bisagno V, Mahaffey S, Lee S, Garcia-Rill E, 2018 Class II histone deacetylases require P/Q-type Ca^{2+} channels and CaMKII to maintain gamma oscillations in the pedunculopontine nucleus. Sci. Rep. 8, 13156. 10.1038/s41598-018-31584-2.

Urbano FJ, Bisagno V, Garcia-Rill E, 2019 Gamma oscillations in the pedunculopontine nucleus are regulated by F-actin: Neuroepigenetic implications. Am. J. Physiol. Cell Physiol. In press. 10.1152/ajpcell.00374.2019.

Wang HL, Morales M, 2009 Pedunculopontine and laterodorsal tegmental nuclei contain distinct populations of cholinergic, glutamatergic and GABAergic neurons in the rat. Eur. J. Neurosci. 29, 340–358. 10.1111/j.1460-9568.2008.06576.x. [PubMed: 19200238]

Ye M, Hayar A, Strotman B, Garcia-Rill E, 2010 Cholinergic modulation of fast inhibitory and excitatory transmission to pedunculopontine thalamic projecting neurons. J. Neurophysiol. 103, 2417–2432. 10.1152/jn.01143.2009. [PubMed: 20181729]

Highlights

- HDAC class IIa inhibitors (acutely, *i.p.*) blunted PPN oscillations at gamma band.
- HDAC class I inhibitors (100mg/kg; *i.p.*) increased PPN gamma band oscillations.
- We suggest the existence of a physiological HDAC class I/IIa balance in the PPN.

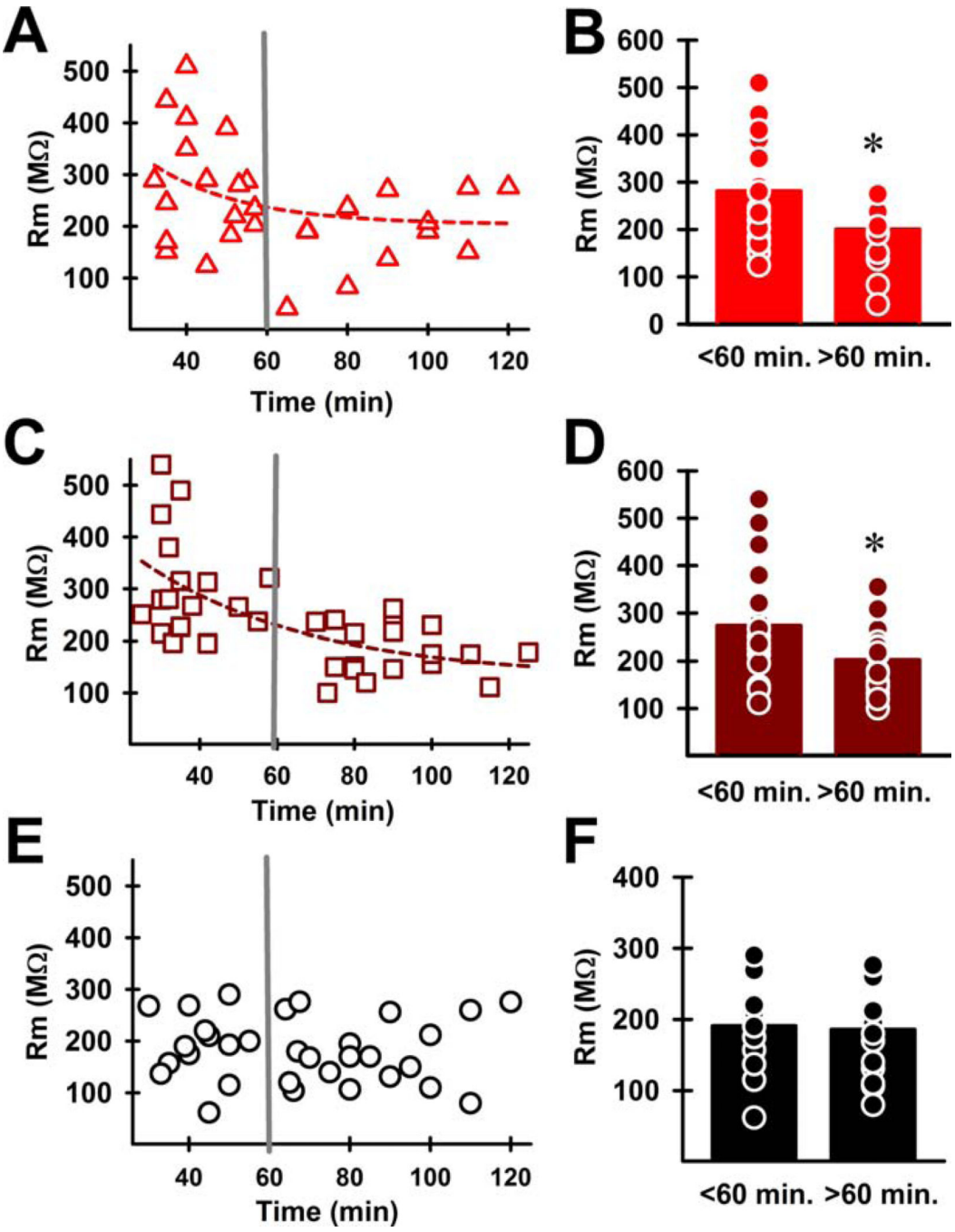

Figure 1. Time-course of membrane resistance (Rm) recorded *in vitro* in PPN neurons after *in vivo* administration of MC1568 (20 mg/Kg) and Trichostatin-A (TSA, 20 mg/Kg).

A. Time course of a specific HDAC IIa inhibitor, MC1568 (20 mg/Kg, *i.p.*) *in vitro* effect on Rm (MΩ). Higher Rm values for MC1568 treated animals when PPN neurons were recorded from 30 minutes (i.e., 20 incubation time +10 min, required to transfer slices to the recording chamber and start *in vitro* recordings) vs 60 minutes after cutting slices in the presence of SB+TTX. Resistance values were fitted to an exponential decay (equation: $Rm=(Rm)o + a*\exp^{(-time/\tau)}$). Fitting results showed a τ=22 min. **B.** Significantly higher

mean Rm values 60 minutes before vs after of *in vitro* recordings in MC1568 treated rats. *, P<0.05; <60 min, Rm=281±26 MΩ, n=16 cells; >60 min, Rm=192±28 MΩ, n=13 cells; One way ANOVA, F(1,28)=4.25, post hoc Tukey's test, q=2.9; P=0.04. **C.** Rm from Trichostatin-A (TSA, 20 mg/Kg, *i.p.*) values were fitted to an exponential decay, following a τ=44 min. **D,** significantly higher mean Rm values 60 min before vs after of *in vitro* recordings in TSA (20 mg/Kg; *i.p.*) treated rats. *, P<0.05; <60 min, Rm=273±26 MΩ, n=20 cells; >60 min, Rm=202±14 MΩ, n=22 cells; One way ANOVA, F(1,41)=5.82, post hoc Tukey's test, q=3.4; P=0.02. **E**. No exponential decay was observed in the time course of Rm (MΩ) values of PPN neurons recorded from Vehicle treated rats. **F.** No significant changes were observed on mean Rm values over the same time periods after Vehicle: <60 min; Rm=185.9±21.4 MΩ, n=13 cells; >60 min; Rm=217.4±17.1 MΩ, n=14 cells; One way ANOVA, F(1,26)=0.004, P=0.9.

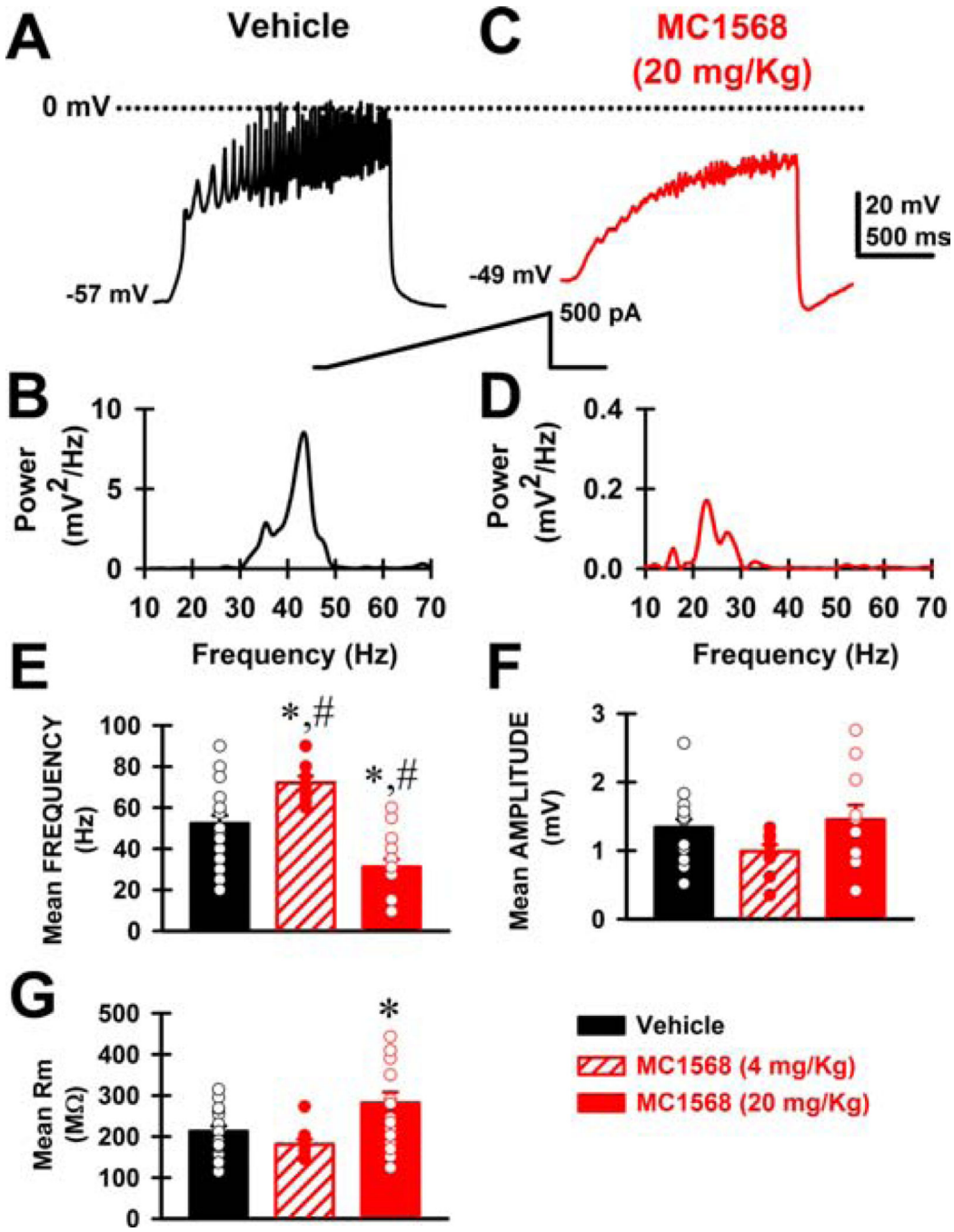

Figure 2. Effects of *in vivo* MC1568 administration on PPN gamma oscillations.

A, B. Ramp-induced oscillations and power spectrum, respectively, from a neuron recorded in PPN slices in the presence of SB+TTX 4 hr and 30 min after intraperitoneally (*i.p.*) injecting a rat with Vehicle. Note the oscillations in A and the power spectrum in B showing gamma frequency oscillations. **C, D.** Same as **A, B** for a 20 mg/Kg (*i.p.*) treated rat. Note how MC1568 reduced both amplitude (C) and frequency (D) of oscillations. **E.** Bar graph representing mean oscillation frequency for PPN neurons from Vehicle (black bar, n=24 cells), MC1568 treatments at a low dose (dashed red bar; 4 mg/Kg, *i.p.*; n=11 cells) or high

dose (red bar; 20 mg/Kg, *i.p.*; n=16 cells). * p<0.05, One way ANOVA, F(2,50)=21.1, p<0.001; *post hoc Tukey's test*, MC1568 (4 mg/Kg) *vs* Vehicle, q=4.7, p<0.005; MC1568 (20 mg/Kg) *vs* Vehicle, q=5.7, p<0.001, # P<0.05, *post hoc Tukey's test*, MC1568 (4 mg/Kg) *vs* MC1568 (20 mg/Kg), q=9.1, p<0.001. **F.** Bar graph representing mean amplitude of oscillations in PPN neurons from Vehicle (black bar; n=17 cells), MC1568 low dose (dashed red bar; 4 mg/Kg, *i.p.*; n=10 cells), and MC1568 treated (red bar; 20 mg/Kg, *i.p.*; n=11 cells) animals. No statistically different amplitudes were observed when comparing all groups using one-way ANOVA (F(2,37)=2.0, p=0.14). **G.** Bar graph representing mean input resistance (Rm) for PPN neurons from Vehicle (black bar; n=22 cells), MC1568 at a low dose (dashed red bar; 4 mg/Kg, *i.p.*; n=10 cells), or high dose of (red bar; 20 mg/Kg, *i.p.*; n=17 cells). * p<0.05, One way ANOVA, F(2,48)=6.3, p=0.004; *post hoc Tukey's test*, MC1568 (20 mg/Kg) *vs* vehicle, q=3.9, p=0.02; MC1568 (20 mg/Kg) *vs* MC1568 (4 mg/Kg), q=4.6, p=0.006, MC1568 (4 mg/Kg) *vs* Vehicle, q=1.5, p=0.6. Brackets in all bar graphs represent the number of cells recorded.

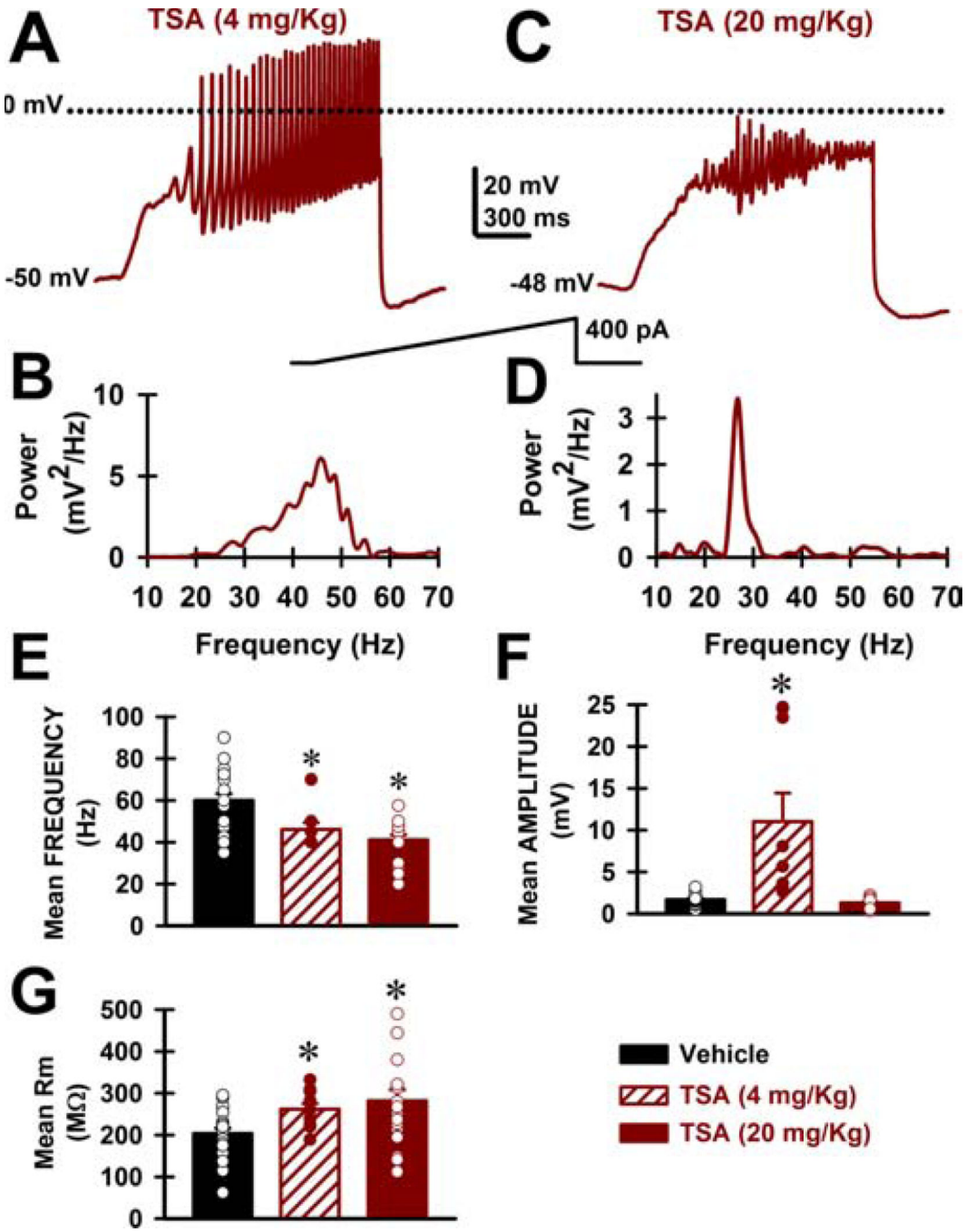

Figure 3. Effects of *in vivo* trichostatin A (TSA) administration on PPN gamma oscillations.

A, B. Ramp-induced oscillations (**A**) and power spectrum (**B**), respectively, from a neuron recorded in PPN slices in the presence of SB+TTX 4 hr after intraperitoneally (*i.p.*) injecting the rat with trichostatin A (TSA, 4 mg/Kg). **C, D.** Same as panels **A, B** for a TSA (20 mg/Kg) treated rat. Note how systemic treatment with 20 mg/Kg TSA notably reduced the amplitude and frequency of oscillations. **E.** Bar graph representing mean frequency for PPN neurons from Vehicle (black bar; n=22 cells), TSA low dose (dashed brown bar; 4 mg/Kg, *i.p.*; n=9 cells), and TSA high dose treatments (filled brown bar; 20 mg/Kg, *i.p.*; n=16 cells).

* P<0.05, One way ANOVA, F(2,46)=12.3 p<0.001; *post hoc Tukey's test*, TSA (4 mg/Kg) *vs* vehicle, q=4.0, p=0.02; TSA (20 mg/Kg) *vs* Vehicle, q=6.8, p<0.001. No significantly different frequencies were observed comparing TSA low (4 mg/Kg) *vs* TSA high (20 mg/Kg) doses, q=1.4, p=0.6. **F.** Bar graph representing mean oscillation amplitude for PPN neurons from Vehicle (black bar; n=20 cells), TSA low dose (dashed brown bar; 4 mg/Kg, *i.p.*; n=11 cells), and TSA high dose (solid brown bar; 20 mg/Kg, *i.p.*; n=19 cells) treatments. Significantly higher amplitudes were observed for TSA low dose (4mg/Kg) treatment. * p<0.05, One-way ANOVA, F(2,39)=21.9, p<0.001. *post hoc Tukey's test*, TSA (4 mg/Kg) *vs* Vehicle, q=7.8, p<0.001; TSA low dose (4 mg/Kg) *vs* TSA high dose (20 mg/Kg), q=8.9, p<0.001. **G.** Bar graph representing mean input resistance (Rm) for PPN neurons from Vehicle (black bar), TSA low dose (dashed brown bar; 4 mg/Kg, *i.p.*), and TSA high dose (solid brown bar; 20 mg/Kg, *i.p.*) treatments. * p<0.05, One way ANOVA, F(2,49)=4.4, p=0.02; *post hoc Tukey's test*, TSA (20 mg/Kg) *vs* Vehicle, q=3.9, p=0.02; One way ANOVA, F(1,30)=7.5, p=0.01; *post hoc Tukey's test*, TSA low dose (4 mg/Kg) *vs* Vehicle, q=3.9, p=0.01. No significant differences were observed on mean Rm comparing TSA high dose (20 mg/Kg) *vs* TSA low dose (4 mg/Kg), *post hoc Tukey's test*, q=4.0, p=0.9.

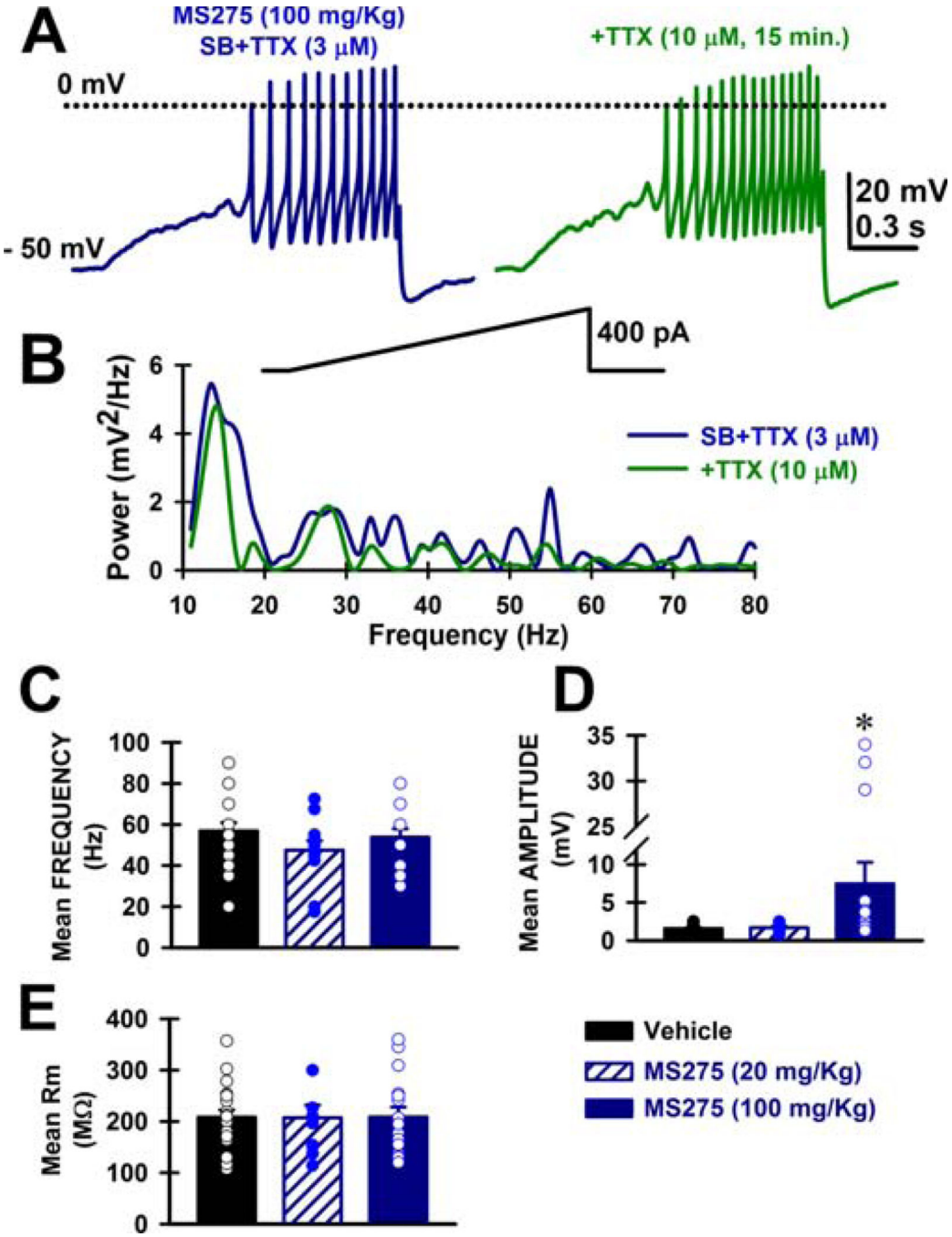

Figure 4. Effects of *in vivo* MS275 administration on PPN gamma oscillations.

A. Ramp-induced oscillations in the presence of SB+TTX (3 μM) and 15 min after SB+TTX (10 μM). **B.** Power spectrum corresponding to the same cell shown in **A**. **C.** Bar graph representing mean oscillation frequency for all PPN neurons recorded from Vehicle (black bar; n=19 cells), MS275 low dose (dashed blue bar; 4 mg/Kg, *i.p.*; n=12 cells), and MS275 middle dose (solid blue bar; 20 mg/Kg, *i.p.*; n=16 cells) treatments. No significant differences were observed (One Way ANOVA, F(2,46)=1.1, p=0.3). **D.** Bar graph representing mean oscillation amplitude for PPN neurons from Vehicle (black bar; n=17

cells), MS275 middle dose (dashed blue bar; 20 mg/Kg, *i.p.*; n= 10 cells), and MS275 high dose (solid blue bar; 100 mg/Kg, *i.p.*; n=17 cells) treatments. Significantly higher oscillation amplitudes were observed for TSA high dose (100 mg/Kg) treatment. One-way ANOVA, $F(2,43)=4.4$, $p=0.02$. * $P<0.05$, *post hoc Tukey's test*, MS275 (100 mg/Kg) *vs* Vehicle, $q=3.9$, $p=0.02$. **E.** Bar graph representing mean input resistance (Rm) for PPN neurons from Vehicle (black bar; n=19 cells), MS175 low dose (dashed blue bar; 4 mg/Kg, *i.p.*; n=12 cells), and MS275 middle dose (solid blue bar; 20 mg/Kg, *i.p.*; n=16 cells) treatments. No significant differences were observed (One Way ANOVA $F(2,46)=0.008$, $p=0.9$).

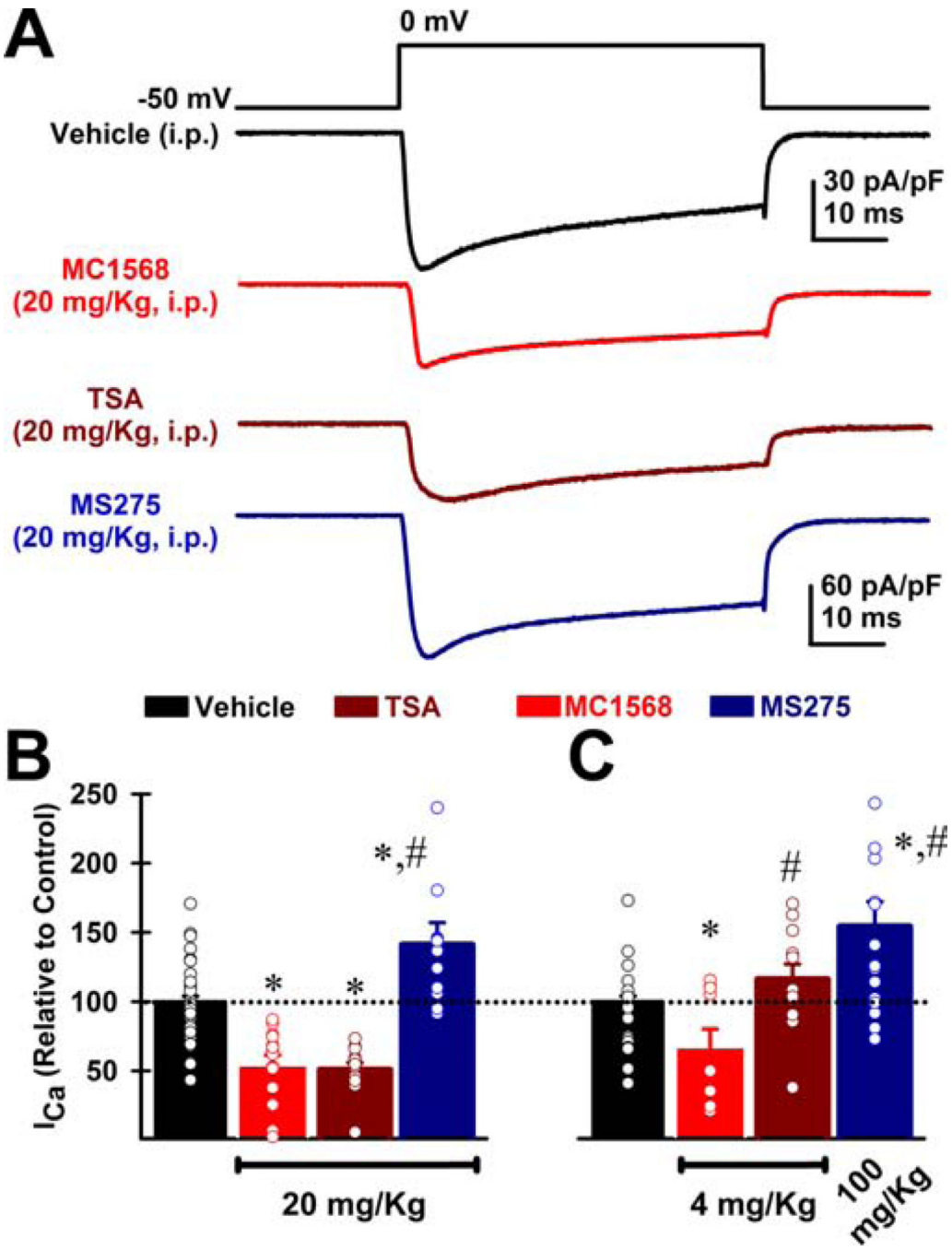

Figure 5. Effects of *in vivo* administration of MC1568, TSA, and MS275 on voltage-dependent Ca^{2+} currents (I_{Ca}) in PPN neurons.

A. Representative I_{Ca} (current density values, pA/pF) recordings in PPN neurons elicited by a 50 msec long depolarizing square step from a holding potential of −50 mV to 0 mV after Vehicle (black record), MC1568 (red record), TSA (brown record), and MS275 (blue record) treatments. **B.** Percent change of I_{Ca} amplitude after Vehicle (black bar; n=39 cells), 20 mg/Kg MC1568 (red bar; n=17 cells), 20 mg/Kg TSA (brown bar; n=12 cells), and 20 mg/Kg MS275 treatments (blue bar; n=11 cells). One Way ANOVA, $F(3,77)=24.3$, $p<0.001$.

* p<0.05; I_{Ca} comparing all treatments; *post hoc Tukey's test*, 20mg/Kg MC1568 *vs* Vehicle, q=8.1, p<0.001; 20 mg/Kg TSA *vs* Vehicle, q=6.8, p<0.001; 20 mg/Kg MS275 *vs* Vehicle, q=4.3, p=0.016. # P<0.05 *post hoc Tukey's test*, 20 mg/Kg *MS275 vs* 20 mg/Kg MC1568, q=9.9, p<0.001; 20 mg/Kg *MS275 vs* 20 mg/Kg TSA, q=8.9, p<0.001. **C.** Percent change of I_{Ca} amplitude after Vehicle (black bar; n=16 cells), 4 mg/Kg MC1568 (red bar; n=9 cells), 4 mg/Kg TSA (brown bar; n=11 cells), and 100 mg/Kg MS275 treatments (blue bar; n=15 cells). One Way ANOVA, F(3,50)=8.0, p<0.001. * p<0.05; I_{Ca} comparing all treatments; *post hoc Tukey's test*, 100 mg/Kg MS275 *vs* Vehicle, q=4.3, p<0.01; MC1568 4 mg/Kg *vs* Vehicle, q=4.1, p=0.03. No statistically significant differences were observed comparing 4 mg/Kg TSA *vs* Vehicle, q=1.4, p=0.7. # p<0.05 *post hoc Tukey's test*, 100 mg/Kg MS275 *vs* 4 mg/Kg MC1568, q=6.8, p<0.001; 4 mg/Kg TSA *vs* 4 mg/Kg MC1568, q=5.0, P=0.005; 100 mg/Kg MS275 *vs* Vehicle, q=4.3, p<0.005. No statistically significant differences were observed comparing 20mg/Kg *vs* 100 mg/Kg MS275, one way ANOVA, F(1,25)=0.02, p=0.9.

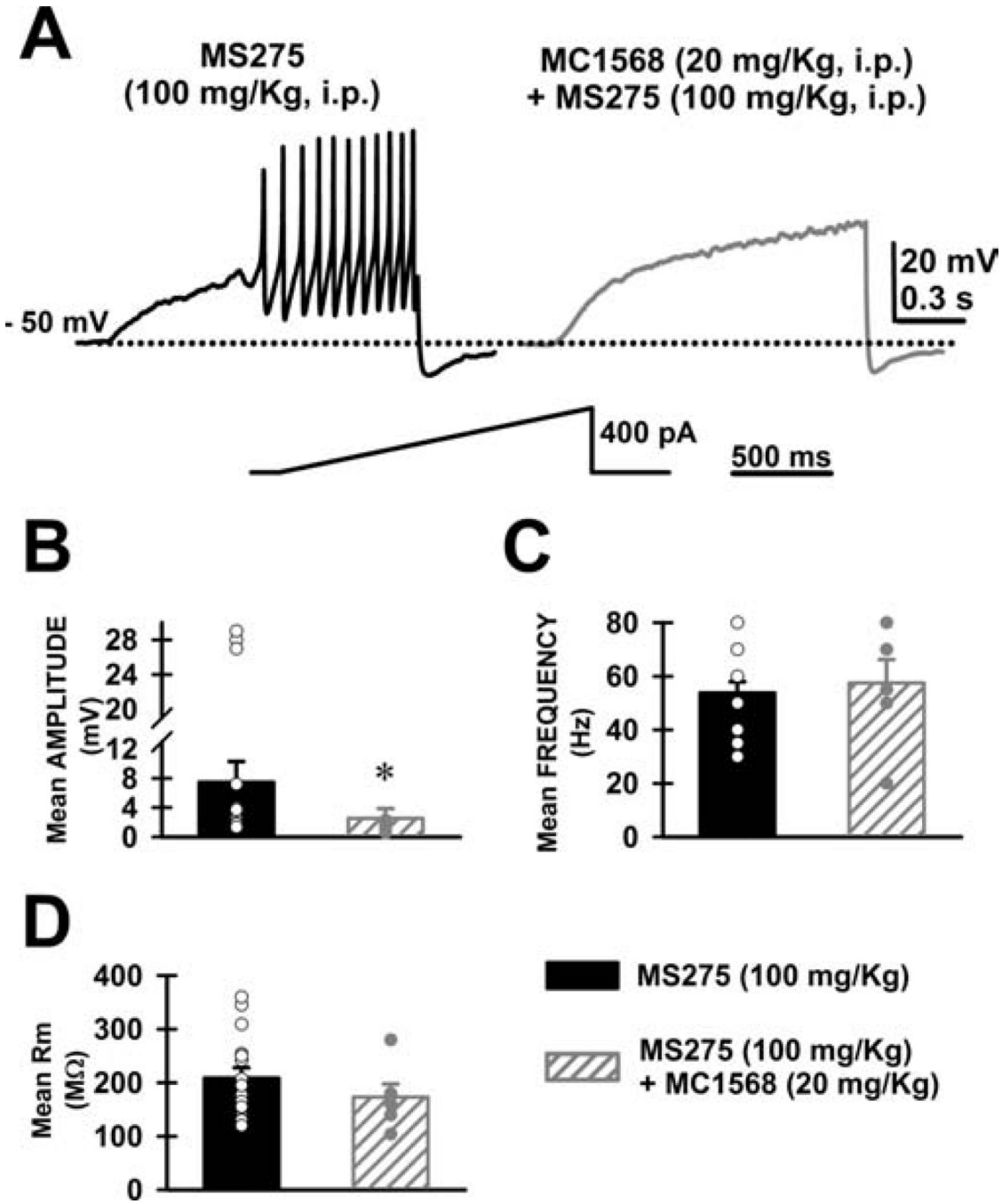

Figure 6. Effects of *in vivo* MS275+MC1568 administration on PPN gamma oscillations.

A. Representative ramp-induced oscillations of PPN neurons from a rat treated systemically with MS275 (100 mg/Kg, *i.p.*; left panel) or MS275+MC1568 (100 mg/Kg+20 mg/Kg; right panel) in the presence of SB+TTX. **B.** Bar graph representing mean amplitude of oscillations in PPN neurons from a MS275 (black bar; 100 mg/Kg; n=17 cells) or a MS275+MC1568 (100 mg/Kg+20 mg/Kg; grey bar; n=6 cells) treated rat. Significantly lower amplitudes were observed for the combination MS275+MC1568 treatment. * P<0.05, One-way ANOVA, F(1,22)=7.3, p=0.01, *post hoc Tukey's test*, MS275+MC1568 *vs* MS275, q=3.8, p=0.01. **C.**

Bar graph representing mean frequency of oscillations for PPN neurons from a MS275 (black bar; 100 mg/Kg; n=16 cells) or a MS275+MC1568 (100 mg/Kg+20 mg/Kg; grey bar; n=6 cells) treated rat. No significant differences were observed (One Way ANOVA, $F(2,21)=0.2$, $p=0.7$). **D.** Bar graph representing mean input resistance (Rm) for PPN neurons from a MS275 (black bar; 100 mg/Kg; n=16 cells) or a MS275+MC1568 (100 mg/Kg+20 mg/Kg; grey bar; n=6 cells) treated rat. No significant differences were observed (One Way ANOVA, $F(2,21)=1.0$, $p=0.3$).